Cycles of self-pulsations in a photonic integrated circuit

Andreas Karsaklian Dal Bosco,[1] Kazutaka Kanno,[1,2] Atsushi Uchida,[1] Marc Sciamanna,[3]
Takahisa Harayama,[4,5] and Kazuyuki Yoshimura[4]

[1]*Department of Information and Computer Sciences, Saitama University, 255 Shimo-Okubo Sakura-ku, Saitama City, Saitama 338-8570, Japan*

[2]*Department of Electronics Engineering and Computer Science, Fukuoka University, 8-19-1 Nanakuma, Johnan-ku, Fukuoka 814-0180, Japan*

[3]*Centrale-Supélec, OPTEL Research Group, Laboratoire Matériaux Optiques, Photoniques et Systèmes (LMOPS) EA-4423, 2 rue Édouard Belin F-57070 Metz, France*

[4]*NTT Communication Science Laboratories, NTT Corporation, 3-1 Morinosato, Wakamiya, Atsugi-Shi, Kanagawa 243-0198, Japan*

[5]*Department of Applied Physics, School of Advanced Science and Engineering, Faculty of Science and Engineering, Waseda University 3-4-1 Okubo, Shinjuku-ku, Tokyo 169-8555, Japan*

(Received 26 March 2015; published 7 December 2015)

We report experimentally on the bifurcation cascade leading to the appearance of self-pulsation in a photonic integrated circuit in which a laser diode is subjected to delayed optical feedback. We study the evolution of the self-pulsing frequency with the increase of both the feedback strength and the injection current. Experimental observations show good qualitative accordance with numerical results carried out with the Lang-Kobayashi rate equation model. We explain the mechanism underlying the self-pulsations by a phenomenon of beating between successive pairs of external cavity modes and antimodes.

DOI: 10.1103/PhysRevE.92.062905 PACS number(s): 05.45.−a, 42.82.Et, 42.60.Rn

I. INTRODUCTION

Semiconductor lasers subjected to optical feedback from an external cavity are well-known examples of nonlinear systems showing rich dynamics [1,2]. A common effect of the feedback is the route to chaos, which begins with the appearance of fluctuations at the relaxation oscillation frequency followed by a succession of bifurcations to diverse nonlinear dynamics and eventually chaos [3–7]. We focus in this paper on the onset of one kind of such nonlinear dynamics, self-pulsation. The term self-pulsation refers to a dynamical state in which the laser exhibits regular pulses repeating at a precise frequency. It corresponds to stable harmonic oscillations of the emitted intensity versus time, also referred to as period 1 [8–12]. In this case the laser radio-frequency (RF) spectrum displays a sharp peak corresponding to the pulsing frequency, followed by smaller peaks repeating at its multiples.

The bifurcation of a laser diode output to self-pulsation owing to time-delayed feedback has been already addressed in the early stage of laser development [13]. Since then several mechanisms have been identified for self-pulsation in various configurations. In a laser diode with optical feedback, phase locking between external cavity modes results in the emission of pulses at a frequency equal to the external cavity frequency (f_{cav}) [14,15]. Fundamental and superharmonic self-pulsations (where the pulsing frequency corresponds to multiples of the external cavity frequency: $f = nf_{\mathrm{cav}}$) have been reported in the particular configuration of a laser diode with phase-conjugate feedback [16].

The bifurcation to self-pulsation in a laser diode with short external cavity has been reported theoretically, in which self-pulsation is generated from a beating between an external cavity mode and an external cavity antimode. External cavity modes and antimodes are respectively stable and unstable solutions of steady intensity of the laser rate equations and are generated by pairs [17]. As the feedback strength is increased, the gains of the various modes and antimodes vary and eventually two of them can reach close values. At that point, a bridge connecting two Hopf bifurcations, one located on a mode and the other on an antimode of a different pair of mode/antimode, can be built. Along this bridge, a self-pulsing dynamics emerges at the frequency of the beating between the connected mode and antimode [11,15,18–21]. Since the frequency distribution of the external cavity modes and the antimodes depends on f_{cav}, the frequency of the beating dynamics, i.e., the self-pulsation, also scales with the change of external cavity time delay. In this paper we present an experimental observation of the bifurcation scenario showing this phenomenon of self-pulsation originated by a beating between successive pairs of modes and antimodes, and we discuss the evolution of the pulsing frequency as the feedback strength increases.

Although numerous theoretical contributions have discussed self-pulsation from mode-antimode beating, experimental observations still remain scarce. Even though mode beating is predicted as a stable solution of the commonly used Lang-Kobayashi model, the likelihood to see this phenomenon is strongly dependent on the external cavity length. A distinction between long and short cavity regimes is done on the basis of a difference of time scale between the laser relaxation oscillation frequency f_{RO} and the external cavity frequency f_{cav}. A laser operates in a short cavity regime when $f_{\mathrm{cav}} > f_{RO}$ and in a long cavity regime when $f_{\mathrm{cav}} < f_{RO}$ [22,23].

It is difficult to observe self-pulsation based on mode-antimode beating in long external cavity configurations since the external cavity modes are distributed very closely one to another in the phase space. As a result, a beginning of beating between two of them would quickly give way to a chaotic itinerancy involving many other modes, thus leading the laser to a dynamics of a complex frequency content or chaos. Therefore, mode beating between two external cavity modes is more likely to be seen in configurations of short external cavities in which the frequency spacing is large and the dynamics involves few modes.

Recently the interest for nonlinear dynamics in short cavity laser systems and monolithic photonic integrated circuits (PICs) has considerably grown. Due to their compactness and their high phase stability, many contributions have discussed the suitability of PICs for chaos generation or laser coupling in applications in the fields of fast random bit generation or telecommunications [24–29]. Initially reported theoretically in 1994 [15], self-pulsation later has been analyzed experimentally in lasers with ultrashort external cavity (hundreds of micrometers) [11,21]. Experiments revealed self-pulsations reaching several tens of GHz. Discussions of the influence of active or passive feedback, the phase modulation, and a proposition of an enhanced system of equation taking into account the nonlinear dynamics of the active external cavity, namely the traveling wave equations (TWEs) [30,31] allowed researchers to predict the pulsing frequencies with better compliance with the experiment.

In spite of these works reporting on self-pulsation in laser diode with ultrashort time delay, several issues remain regarding, e.g., a detailed experimental bifurcation analysis of self-pulsing dynamics and the evolution of the corresponding frequency versus the laser parameters. Although experiments that have been carried out in a laser with ultrashort cavity [11,21] mention that self-pulsations originate from a beating between modes and antimodes, the sequence of bifurcation between successive pulsing states is not detailed. Although both the short cavity regime (where the external cavity length reaches some millimeters) and the ultrashort cavity regime (where the external cavity length is limited to hundreds of micrometers) comply with the $f_{\mathrm{cav}} > f_{RO}$ condition, one can expect that such a discrepancy in the cavity length induces different dynamical evolutions.

There have been reports addressing the question of how the waveforms corresponding to quasiperiodic or chaotic dynamics evolve in the transition from long to short external cavity has been addressed, e.g., very recently in a four-section integrated laser diode [32]. Dynamics corresponding to the so-called regular pulse package of the short cavity regime [33] evolve to strongly irregular chaotic pulsing when sweeping the relaxation oscillation frequency across the external cavity frequency. The way these dynamics bifurcate from self-pulsation has been studied in detail in short-cavity laser diodes in free space [34] but not in the case of PIC.

Understanding the bifurcations to self-pulsation is therefore necessary to control the dynamics and take better advantage of PICs' rich capabilities for signal applications. An interesting application of pulsing states that has been drawing interest recently is microwave photonic technology, which aims at generating optical signals at several tens of GHz to perform data transmission [35–38]. The commonly used technology mostly relies on laser coupling by optical injection or optoelectronic feedback [39–41]. Making use of the advantages of a PIC to generate a source of microwave optical signals is a challenge that will certainly be faced in the near future.

In this paper we bring a contribution composed of a detailed experimental scenario showing how a laser diode can switch from successive steady states to self-pulsation and back to steady state. We study the case of a laser diode in a short external cavity regime and integrated on a PIC. We show that the dynamics is obtained from a cascade of bifurcations leading to steady states, self-pulsing states, and quasiperiodicity as the feedback strength varies. For theoretical insight, we provide simulated results which enable us to confirm that the underlying phenomenon at the origin of self-pulsation is indeed a beating between external cavity modes and antimodes. Moreover, we illustrate the relationship between the mode distribution and the self-pulsing frequency. The cascade of bifurcations associated with the qualitative change of dynamics is unveiled as well as the respective influences of the feedback strength and the laser injection current on the pulsing frequencies.

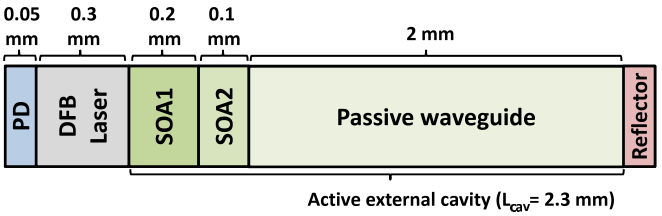

FIG. 1. (Color online) Photonic integrated circuit. PD: photodiode, DFB laser: distributed feedback laser, SOA: semiconductor optical amplifier.

II. EXPERIMENTAL SETUP

Our PIC is schematically described in Fig. 1. It consists of a distributed feedback semiconductor laser (wavelength of 1537 nm) bounded by a photodiode (PD) and a 2.3-mm-long active external cavity. This cavity is composed of two independent semiconductor optical amplifiers (SOA1 and SOA2) and a passive waveguide ended by a reflector on which a high-reflectivity coating has been applied. The amplified feedback strength is adjusted by the injection currents of the SOAs. We keep the injection current of SOA2 constant ($J_{SOA2} = 5.0$ mA) and therefore change the feedback strength by means of J_{SOA1} only. The whole experimental setup is presented in Fig. 2. We estimate that f_{cav} is close to 17 GHz from measurements on an RF spectrum analyzer. We also measured the relaxation oscillation frequency of our laser, which ranges from 2.3 to 7.4 GHz according to its injection current. This confirms the fact that we work in a short external cavity configuration, since $f_{\mathrm{cav}} > f_{RO}$.

III. EXPERIMENTAL EVIDENCE OF SELF-PULSATION IN PIC

Figure 3 displays temporal and spectral illustration of the experimental transition from a steady state to self-pulsing

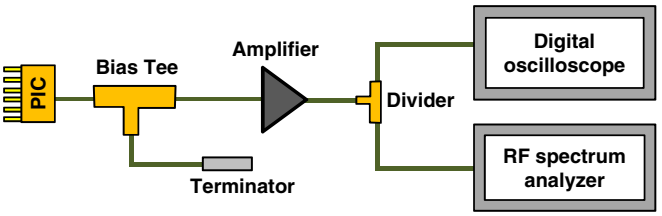

FIG. 2. (Color online) Experimental setup. The electrical output signal provided by the photodiode embedded in the PIC is amplified and directed to a digital oscilloscope (Tektronik DPO73304D, 33 GHz bandwidth, 50 GS/s) and a RF spectrum analyzer (Agilent N9010A, 44 GHz bandwidth).

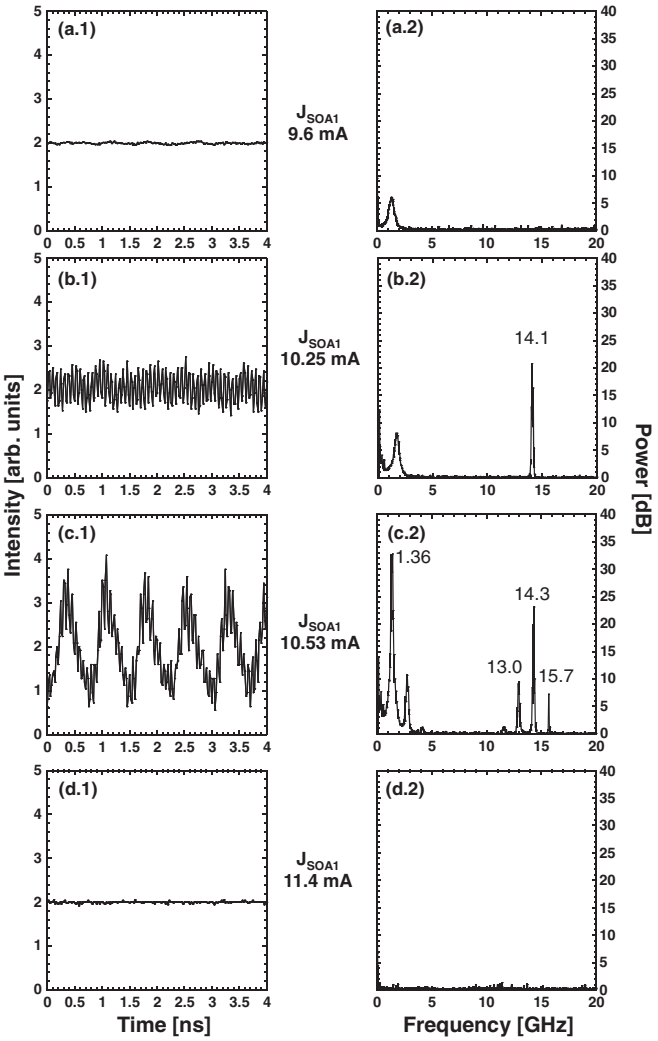

FIG. 3. Experimental observation of self-pulsing dynamics when the injection current J/J_{th} is equal to 1.0. Each line corresponds to a different value of the feedback strength J_{SOA1}. The two columns display the related temporal waveforms and RF spectra, in which the electrical noise of the spectrum analyzer has been subtracted. The values reported above the peaks correspond to their positions in GHz.

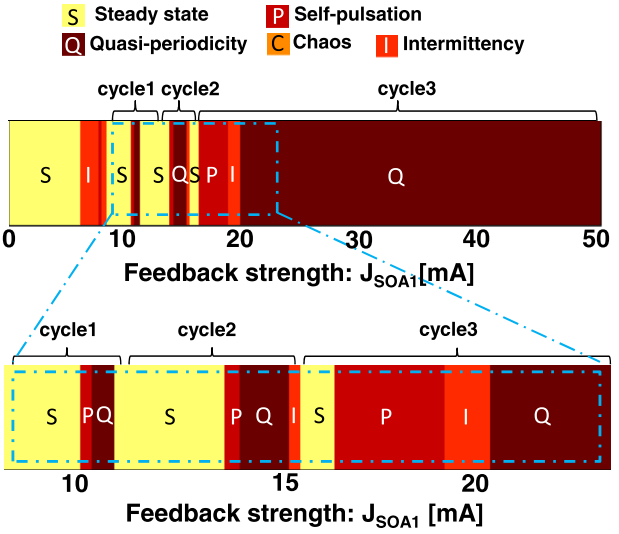

FIG. 4. (Color online) Experimental bifurcation diagram showing three dynamical cycles of self-pulsations seen when increasing the feedback strength J_{SOA1} for a value of the laser injection current J/J_{th} fixed to 1.0. The colors and letters correspond to different dynamics: yellow (S) is steady state, dark red (P) is self-pulsation, brown (Q) is quasiperiodicity. Orange (C) and red (I) represent chaotic and intermittent regimes, which are not discussed here. The region labeled *cycle 1* corresponds to the scenario presented in Fig. 3.

state as the feedback strength, adjusted by the injection current in SOA1 (J_{SOA1}), is increased. The laser injection current is indicated by its normalized value with respect to threshold J/J_{th}, where $J_{th} = 13.0$ mA. The experimental results presented in Fig. 3 were obtained for $J/J_{th} = 1.0$. The scenario unfolds as follows.

First, the laser is in a steady state, thus exhibiting constant optical output power [Fig. 3(a.1)]. For a certain value of the feedback strength, this steady state gives way to self-pulsation; i.e., the temporal waveform shows harmonic oscillations [Fig. 3(b.1)] at the frequency of 14.1 GHz. If the feedback strength is further increased, a new frequency rises upon the harmonic background, inducing a transition to quasiperiodicity [Fig. 3(c.1)]. In the corresponding RF spectrum, several new frequencies appear [Fig. 3(c.2)]. The main one at 14.3 GHz is the reminiscence of the frequency of the self-pulsation. It has been shifted a little bit compared to its position at 14.1 GHz in Fig. 3(b.2) due to the feedback increase. It constitutes the fast dynamics in the time trace, remnant from the previous self-pulsing state. A second peak (along with its multiples) stands in the region of low frequencies (1.36 GHz) and corresponds to the newly emerged slowly varying envelope shaping the time trace in Fig. 3(c.1). Then one can also see peaks at 13.0 GHz and 15.7 GHz, representing the beating between the fast dynamics at 14.3 GHz and the slow one at 1.36 GHz. Quasiperiodicity as seen in Fig. 3(c.1) resembles at first sight the so-called regular pulse packages (RPPs) observed for similar external cavity lengths in free space optical feedback configurations [33,34]. However, as will be discussed in Sec. IV, simulations suggest that this quasiperiodic dynamics involves switching between one external cavity mode and one antimode while the RPP dynamics is a global attractor encompassing a large number of modes. In both cases, however, the repelling trajectories among the modes are responsible for the signature of the low-frequency dynamics seen in the quasiperiodic traces like the one in Fig. 3(c.1). Now, if the feedback strength is increased again, this quasiperiodic dynamics collapses and the laser recovers steady state [Fig. 3(d.1)].

Those three successive behaviors (steady state, self-pulsation, and quasiperiodicity) are part of a dynamical cycle which will be actually repeating itself on the whole range of the feedback strength. Figure 4 represents an experimental bifurcation diagram obtained when varying J_{SOA1} from 0 to 50 mA. In this example, three cycles are visible, since the scenario [steady state (yellow, S); self-pulsation (dark red, P); quasiperiodicity (brown, Q)] is reproduced three times. Although the third one is extended on a quite long feedback span compared to the first two, the dynamical features are

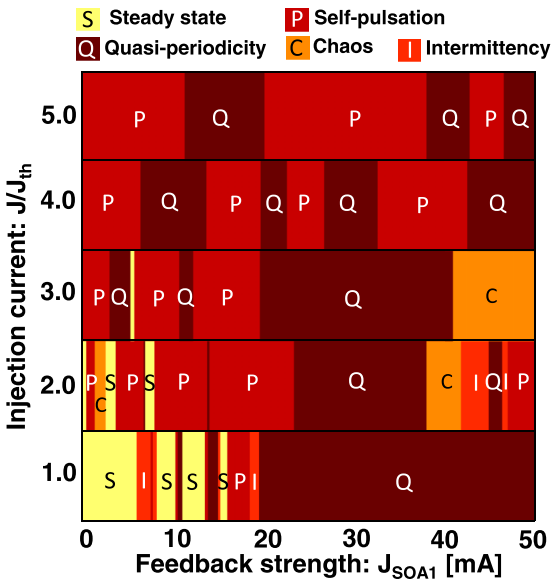

FIG. 5. (Color online) Experimental bifurcation diagrams showing dynamical transitions as the feedback strength J_{SOA1} is increased for values of the laser injection current J/J_{th} varying from 1.0 to 5.0. The colors and letters correspond to different dynamics: yellow (S) is steady state, dark red (P) is self-pulsation, brown (Q) is quasiperiodicity. Orange (C) and red (I) represent chaotic and intermittent regimes, which are not discussed here.

the same. One understands then that the whole dynamical evolution of the laser under the effect of the feedback sketches a cycle which successively reproduces itself.

In order to analyze the influence of the laser injection current on this succession of dynamical cycles, we focus now on the bifurcation diagrams displayed in Fig. 5. The figure is a collection of independent series of dynamical observations carried out by changing the feedback strength (J_{SOA1}) for five different values of the normalized laser injection current (J/J_{th}). Therefore, the values on the vertical axis do not vary continuously. Figure 5 can be seen as a superposition of observations carried out for five different experimental conditions. Comparing to the case we have been discussing for $J/J_{th} = 1.0$, the succession of dynamics as the feedback strength increases is globally the same for all values of J/J_{th}. Nonetheless we can point out that for medium and high values of the injection currents J/J_{th}, the regions corresponding to steady states vanish, and the whole dynamics is mostly governed by regions of self-pulsation and quasiperiodicity visible on larger feedback spans. Therefore the sequence of bifurcations to steady states, self-pulsation, and quasiperiodicity is reduced to bifurcations leading to self-pulsation and quasiperiodicity only. In that case, experimental observations show that quasiperiodicity terminates with a direct transition to the next self-pulsing state. Yet although the steady states may be discarded, the dynamical evolution composed of transitions to successive self-pulsing states through quasiperiodicity is robust to changes of J/J_{th}. It is also worth to mention that the evolution of the feedback spans on which self-pulsation and quasiperiodicity are visible is not simple and does not seem to follow a particular law with J/J_{th}, even though they tend to widen for high currents.

TABLE I. Parameter values in simulations.

Symbol	Parameter	Value
G_N	Gain coefficient	8.40×10^{-13} m^3 s^{-1}
N_0	Carrier density at transparency	1.40×10^{24} m^{-3}
τ	Feedback time delay	59×10^{-12} s
τ_p	Photon lifetime	1.927×10^{-12} s
τ_s	Carrier lifetime	2.04×10^{-9} s
τ_{in}	Internal cavity round-trip time	8.0×10^{-12} s
R_2	Laser facet reflectivity	0.556
α	Line width enhancement factor	3.0
N_{th}	Carrier density at threshold	2.018×10^{24} m^{-3}
$j = J/J_{th}$	Normalized injection current	1.5
ϵ	Gain saturation coefficient	2.5×10^{-23}

IV. NUMERICAL ANALYSIS

In order to study the theoretical mechanism underlying the experimental observations, we carry out simulations making use of the Lang-Kobayashi rate equations [42–44]:

$$\frac{dE(t)}{dt} = \frac{1}{2}\left[\frac{G_N(N(t)-N_0)}{1+\epsilon E^2(t)} - \frac{1}{\tau_p}\right]E(t) + \kappa E(t-\tau)\cos[\Theta(t)], \quad (1)$$

$$\frac{d\Phi(t)}{dt} = \frac{\alpha}{2}\left\{\frac{G_N[N(t)-N_0]}{1+\epsilon E^2(t)} - \frac{1}{\tau_p}\right\} - \kappa\frac{E(t-\tau)}{E(t)}\sin[\Theta(t)], \quad (2)$$

$$\frac{dN(t)}{dt} = J - \frac{N(t)}{\tau_s} - \frac{G_N[N(t)-N_0]}{1+\epsilon E^2(t)}E^2(t), \quad (3)$$

$$\Theta(t) = \omega\tau + \Phi(t) - \Phi(t-\tau). \quad (4)$$

In these equations N, E, and Φ are, respectively, the carrier density, the electric field amplitude, and the electric field phase. τ and κ represent the feedback delay and strength, α is the line-width enhancement factor, J is the laser injection current, G_N is the gain coefficient, N_0 is the carrier density at transparency, τ_p and τ_s are the photon and carrier lifetime, respectively, and ϵ is the gain saturation coefficient. The delay τ is chosen equal to 59 ps, which corresponds to $f_{\text{cav}} = 17$ GHz, like in our PIC. In the simulations, we use the parameter R to measure the feedback strength. R can be seen as a reflectivity coefficient for the electric field amplitude and is defined by $\kappa = (1 - R_2^2)R/(\tau_{in}R_2)$. In this formula, τ_{in} and R_2 are respectively the photon round-trip time in the laser internal cavity and the amplitude reflectivity coefficient of the laser output facet. The values of the parameters are given in Table I.

The Lang-Kobayashi equations do not take into account the dynamics related to the active external cavity. As a consequence, we have no parameter to model the SOA currents, and the feedback is simply considered as originated from an external mirror of tunable reflectivity bounding a passive external cavity. The reason for this is that our aim is not to produce a detailed and therefore complex model but rather to understand the general mechanism at the origin of self-pulsation. Therefore our theoretical analysis is limited to qualitative comparisons with our experimental

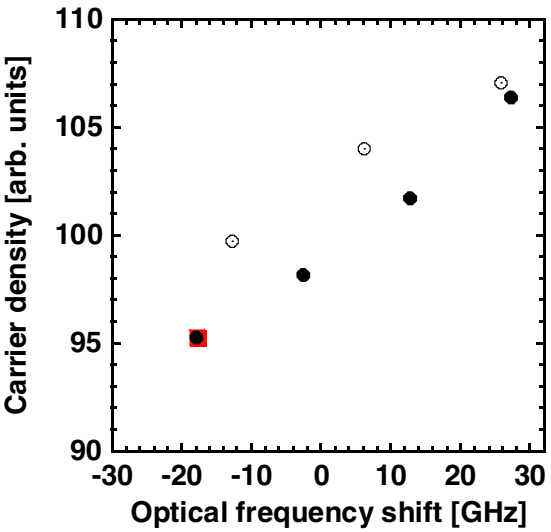

FIG. 6. (Color online) Distribution of the modes (black dots) and antimodes (circles) in the phase space when $R = 0.35$. Y axis is the carrier density (in arbitrary units corresponding to $100N_s/N_{th}$), and X axis is the optical frequency shift with respect to the solitary state [$(\omega_s - \omega)/2\pi$ in GHz]. The red square represents the current steady state.

observations. Yet it is worth mentioning that analyses using the more sophisticated model of the TWE have been carried out, showing good quantitative compliance with experimental observations [11].

Before getting into the dynamical analysis, we present the distribution of the modes and antimodes of our system in the phase space. Modes and antimodes correspond, respectively, to stable and unstable solutions of steady intensity in the Lang-Kobayashi equations [17]. A laser operating in steady state corresponds to stabilization on a mode, while antimodes are unstable steady states. However, as we are about to discuss, modes and antimodes may interact and lead to mode beating dynamics [15,19,20]. We consider the steady-state solutions $E(t) = E_s, \Phi(t) = (\omega_s - \omega)\tau$, and $N(t) = N_s$ in the Lang-Kobayashi equations (1), (2), and (3). Inserting the steady-state solutions into the Lang-Kobayashi equations gives Eqs. (5), (6), and (7) for the steady-state solutions [43,44]:

$$\frac{1}{2}\left[\frac{G_N(N_s - N_0)}{1 + \epsilon E_s^2} - \frac{1}{\tau_p}\right] = -\kappa \cos(\omega_s \tau), \tag{5}$$

$$\omega_s - \omega = -\kappa\sqrt{1+\alpha^2}\sin(\omega_s \tau + \tan^{-1}\alpha), \tag{6}$$

$$N_s = N_{th} + \frac{\epsilon N_{th}(j-1) - 2\kappa\tau_s \cos(\omega_s \tau)}{\tau_s G_N + \epsilon}. \tag{7}$$

In the two-dimensional phase space depicted in Fig. 6, the modes are represented by black dots and the antimodes by circles. The corresponding feedback rate is $R = 0.35$. Their positions are determined by the above-mentioned stationary solutions. For a given stationary solution, the horizontal position (optical frequency shift) corresponds to the value of $(\omega_s - \omega)/2\pi$ in GHz, and its vertical position (normalized carrier density) corresponds to the value of $100N_s/N_{th}$ in arbitrary units. The value of the corresponding electric field amplitude E_s is not used in this two-dimensional distribution of modes and antimodes.

Once the distribution of modes and antimodes is set, the phase trajectory of the laser is sketched in this phase space. It represents the temporal evolution of the carrier density versus the optical frequency shift. The normalized carrier density is calculated as $100N(t)/N_{th}$. The optical frequency shift represents a change from $\omega/(2\pi)$ and is calculated as $[\Phi(t) - \Phi(t-\tau)]/(2\pi\tau)$, which corresponds to a time-averaged value calculated on the time scale of τ. In the example given in Fig. 6, the laser operating point is represented by a red square located on the maximum gain mode (mode for which the value of N_s is minimal), indicating a steady state. As the feedback strength increases, modes and antimodes successively appear in pairs and these new solutions shape an ellipse in the phase plane projection [17]. By contrast to long-cavity configurations in which the number of external cavity modes is large [45], we work here in a short cavity regime where the mode spacing is large and consequently only few modes exist, as can be seen in Fig. 6.

The simulated dynamical scenario corresponding to the experimental one presented in Fig. 3 is shown in Fig. 7. For each value of the feedback strength, we display the temporal waveform [the laser intensity is calculated as $E^2(t)$] and phase trajectory in the phase space. The corresponding RF spectra are given in Fig. 8. The sequence of qualitatively different dynamics starts with a first steady state [Fig. 7(a.1)], corresponding to the laser operating in the maximum gain mode [Fig. 7(a.2)]. When increasing the feedback strength, the system undergoes a Hopf bifurcation leading to a limit cycle attractor, hence to a time-periodic evolution of the output power [Fig. 7(b.1)–7(b.2)]. The self-pulsing frequency (f_{SP}) is 13.3 GHz, which is different from f_{cav}. This was also the case in the experimental observations presented in Fig. 3(b.2). The value of f_{SP} is easily understood from the relative positions of the modes and the antimodes in the phase space. The phenomenon is explained by a beating between one mode (mode 1) and the antimode belonging to the next pair of mode-antimode (antimode 2). This new pair does not yet exist in Fig. 7(a.2) but ends up by appearing as R is increased [Fig. 7(b.2)]. As explained in Ref. [21], new pairs of modes and antimodes are generated as the feedback strength increases. Then beating can happen when a mode and an antimode have approximately the same gain, thus enabling the laser to undergo a bifurcation from the initial steady state to a limit cycle, corresponding to a pulsing dynamics at the frequency difference between the beating external-cavity modes [which can be read on the horizontal axis of Fig. 7(b.2)]. In this example, the frequency separation between mode 1 and antimode 2 is equal to 13.3 GHz. As a consequence, the peak corresponding to the self-pulsing dynamics is located at 13.3 GHz in Fig. 8(a).

Then if R is increased again, the limit cycle corresponding to the self-pulsation bifurcates to a more complex attractor that, in the phase space, involves trajectories close to both the mode and the antimode facing it [mode 1 and antimode 2 in Fig. 7(c.2)]. This new dynamics is representative of quasiperiodicity with the appearance of two incommensurate frequencies [Fig. 7(c.1)]. Indeed, as presented in Fig. 8(b), there is one fast dynamics and one slow dynamics. The fast

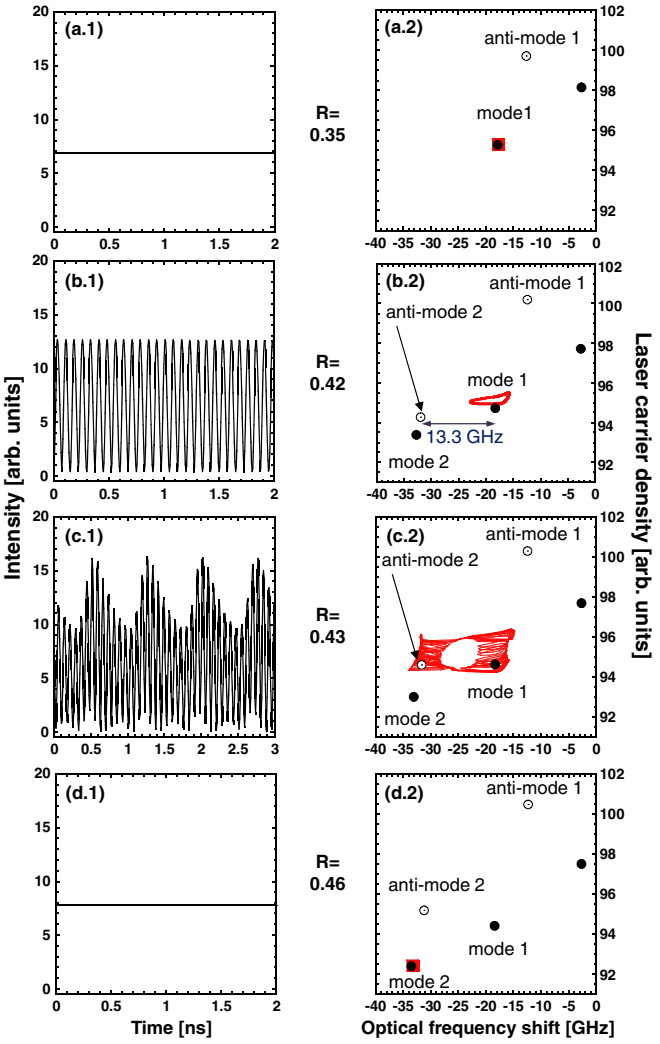

FIG. 7. (Color online) Simulated scenario of self-pulsing dynamics. $J/J_{th} = 1.5$. Each line corresponds to a different value of R. The columns display the related temporal waveforms and phase trajectories in the carrier density-optical frequency shift space. In the phase trajectories, the external cavity modes (antimodes) are represented by dots (circles) and are arbitrarily numbered to illustrate the explanation of the phenomenon of beating. The phase space represented in (a.2) is a zoom on the bottom-left part of Fig. 6.

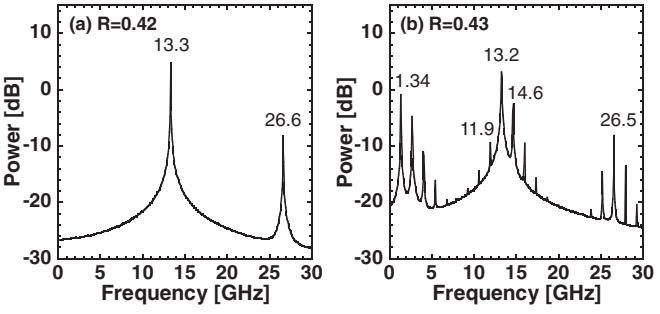

FIG. 8. RF spectra illustrating the frequency content of traces in Figs. 7(b.1) and 7(c.1). The values reported above the peaks correspond to their positions in GHz.

dynamics is represented by the peak at 13.2 GHz, which is actually the peak seen at 13.3 GHz in Fig. 8(a) but slightly shifted. The fast dynamics is therefore still governed by the phenomenon of beating between the mode and the antimode and is represented in the temporal waveform in Fig. 7(c.1) by the fast oscillations. This tiny frequency shift in the RF spectrum is not due to a variation in the positions of the modes and antimodes induced by the increase of R from 0.42 to 0.43 since we found in the simulations that the frequency spacing between given modes and antimodes only increases with the feedback strength. It is rather related to the torus bifurcation itself, which alters a little bit the fundamental pulsing frequency.

The slow dynamics of the quasiperiodicity is represented by the peak at 1.34 GHz in Fig. 8(b). It corresponds to the speed at which the phase trajectory switches between the two attractors located at the vicinities of mode 1 and antimode 2 [Fig. 7(c.2)]. These intermittent jumps between the mode and the antimode represent switches between two solutions having approximately the same gain. In the temporal waveform in Fig. 7(c.1), this second dynamics governs the slowly varying envelope in the laser intensity. Again we can notice in the RF spectrum Fig. 8(b) the peaks corresponding to the beating between the fast and the slow dynamics at 11.9 GHz and 14.6 GHz and on both sides of the peak at 26.5 GHz. Note that the mechanism at the origin of the quasiperiodicity in our case [jumps between attractors located on one mode and one antimode as seen in Fig. 7(c.2)] is different from the global attractor corresponding to a regular itinerancy between many destabilized external cavity modes as reported for the case of RPP [22,33,34].

Eventually, if the feedback strength is increased from that point, those two attractors end up collapsing and the laser gets stabilized to a new steady state [Fig. 7(d.1)]. This transition corresponds more precisely to a saddle-node bifurcation bringing the system to a fixed point on the next mode, represented by a square located on mode 2 in Fig. 7(d.2).

At that stage where the laser has recovered steady state the sequence of bifurcations repeats on the newly born external cavity mode. These simulated results are in very good accordance with the experimental scenario depicted in Fig. 3 from the point of view of both the succession of dynamics and the values of the frequencies at stake in the self-pulsations. This confirms that the self-pulsations seen in the experiment can be explained by the phenomenon of mode beating as we describe here.

The bifurcation scenario yielding the succession of stationary state, self-pulsation, and quasiperiodicity is fundamentally similar to the one reported in Ref. [33], in which RPP dynamics has been reported. The self-pulsing dynamics are originated by a phenomenon of bifurcation bridges inducing a beating between modes and antimodes. The secondary bifurcation from self-pulsation to either pulse packages (in the case of Ref. [33]) involving an itinerancy encompassing many modes and antimodes or the quasiperiodicity reported in the present paper (made of jumps between attractors located on one mode and one antimode) may be due to different experimental conditions.

Now, if the feedback strength increases again, the same three-step scenario will be reproduced, revealing successive

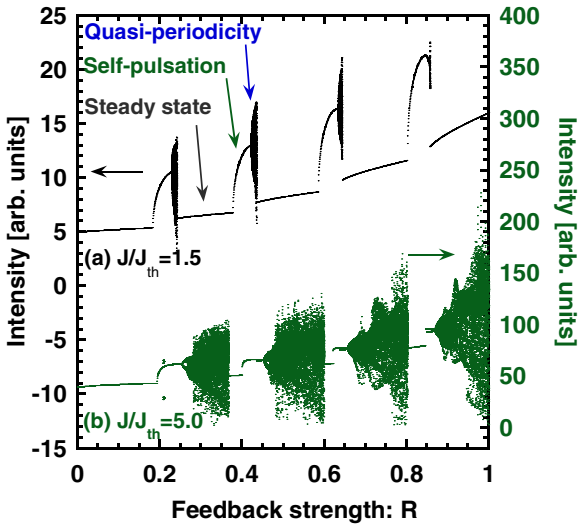

FIG. 9. (Color online) Simulated bifurcation diagrams showing successive cycles, each one constituted of a steady state, self-pulsation, and quasiperiodicity for two values of the laser injection current: $J/J_{th} = 1.5$ (a) and $J/J_{th} = 5.0$ (b). Note that in the case of diagram (b), chaos also occurs.

self-pulsing and quasiperiodic states showing the same qualitative frequency content. This succession of self-pulsations is illustrated in Fig. 9 where numerical bifurcation diagrams are presented on a large span of feedback values for $J/J_{th} = 1.5$ and $J/J_{th} = 5.0$. The scenario illustrated in Fig. 7 corresponds to the region between $R = 0.35$ and $R = 0.46$ in diagram (a). One can clearly see that the sequence of bifurcations repeats itself, revealing regions of self-pulsing states and quasiperiodicity of increasing amplitude. However, by contrast to the experimental bifurcation diagram presented in Fig. 5 in which no particular tendency is denoted, the regions of self-pulsing dynamics seem to shrink as the feedback rate increases. In addition, diagram (b) illustrates the tendency seen in Fig. 5, showing that as the injection current increases, the intervals of feedback in which regions of steady state exist get shorter.

Although the dynamical scenario is qualitatively the same, the comparison between experiment and simulations cannot be carried out much further than phenomenological considerations. We do not find for instance a total disappearance of the regions of steady state when the laser injection current is increased to five times its threshold value. This discrepancy stands probably from the simplicity of the Lang-Kobayashi model, which may be far from the complexity of the actual PIC and which, for instance, does not take into account the dynamics of the photons and the carriers in the SOAs. Nonetheless, the model is satisfactory enough to study the evolution of the pulsing frequency with the feedback strength as we discuss in the next section. Besides being able to understand the phenomenon of beating itself, it is also interesting to carry out a deeper analysis of the evolution of the pulsing frequencies as the feedback increases. Since we know that the frequency spacing between external cavity modes increases with the feedback strength, f_{SP} is expected to evolve alike.

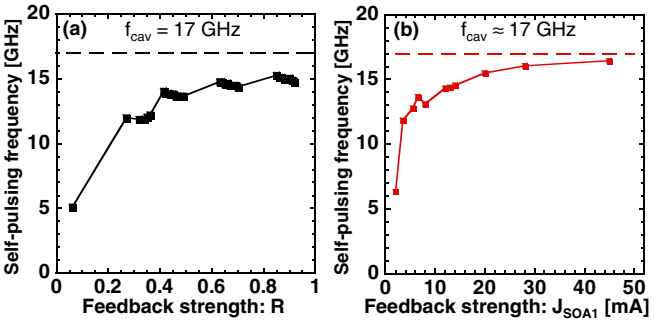

FIG. 10. (Color online) Simulated (a) and experimental (b) evolutions of the self-pulsing frequency as the feedback strength increases when the value of the laser injection current J/J_{th} is fixed to 2.0.

V. EVOLUTION OF THE SELF-PULSING FREQUENCY WITH THE FEEDBACK STRENGTH

In this section we analyze how the pulsing frequencies evolve over a large span of feedback strength and how a dependence on f_{cav} can be established. Figure 10 presents the evolution of the self-pulsing frequencies f_{SP} both measured in the experiment and calculated numerically as the feedback strength increases for the case where $J/J_{th} = 2.0$. The frequencies reported in this figure correspond to f_{SP} when the laser operates in a self-pulsing state. In regions of quasiperiodicity, we considered for f_{SP} the values of the frequency corresponding to the fast-dynamics component in the RF spectrum, as if we were following the position of the peak along the frequency axis. The curves show a general increase of the frequency which is first rapid but gradually slows down. Therefore the larger the feedback strength the higher the pulsing frequency. In Fig. 10(a) a succession of dynamics like the one presented in Fig. 9 is recognizable. In this figure regions of squares close to each other represent regions of self-pulsation and quasiperiodicity, where an oscillating dynamics is visible while regions with no dots correspond to steady states. However, there is a limit value to the increase of f_{SP}. Indeed, we understand from Fig. 10 that this increasing evolution is limited by the value of f_{cav}, which acts as an asymptote to the curves. As a consequence, for a given external cavity length, the self-pulsing states can be expected to pulse at frequencies up to the value of f_{cav}, yet without really reaching it. This evolution of f_{SP} with the feedback strength is related to the evolution of the frequency distribution of the external cavity modes and antimodes, which follows the same tendency with the feedback strength.

VI. INFLUENCE OF THE LASER INJECTION CURRENT ON THE SELF-PULSING FREQUENCY

We saw in Sec. III that the dynamical scenario, composed of cycles of self-pulsation and quasiperiodicity, is robust to changes of the values of the laser injection current. As for the values of the self-pulsing frequencies, their experimental evolution as a function of the feedback strength for different values of J/J_{th} is displayed in Fig. 11. For all values of

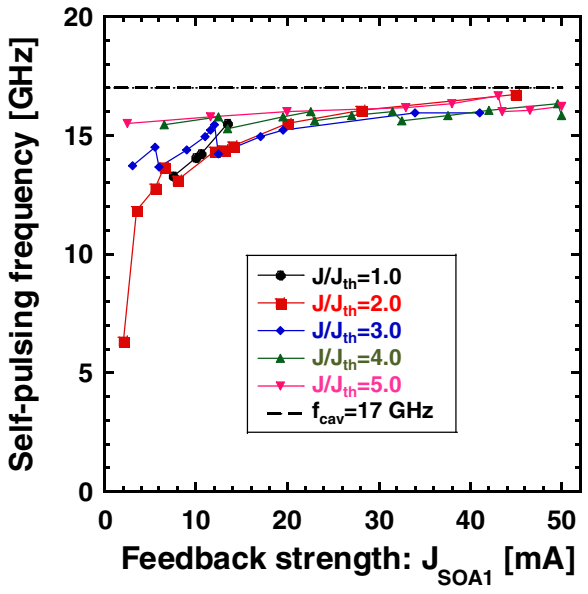

FIG. 11. (Color online) Experimental evolution of the self-pulsing frequencies with the feedback strength (J/J_{SOA1}) for values of the laser injection current J/J_{th} increasing from 1.0 to 5.0.

J/J_{th}, f_{SP} increases with the feedback strength, as seen for the case presented in Fig. 10. An interesting feature is the fact that when comparing the values of the frequencies for given feedback values but for different currents, one clearly sees that the difference is large when the feedback is weak and gets smaller as the feedback strength increases. In other words, the sensitivity of the pulsing frequency to J/J_{th} is higher under weak feedback conditions. This implies that the feedback strength also has an influence on the dependence of f_{SP} on J/J_{th} and L_{cav}. The smaller the feedback rate the higher the influence of the injection current. As a consequence f_{SP} is close to the relaxation oscillation frequency (f_{RO}) and the difference between the values of f_{SP} for different values of J/J_{th} is large. By contrast, when the feedback is strong, f_{SP} is little influenced by the laser injection current and is mostly determined by L_{cav}. As presented in Fig. 11, when J_{SOA1} is large the values of f_{SP} are closer to f_{cav} and little discrepancy is seen in their values when varying J/J_{th}. We checked numerically that the evolution of f_{SP} corresponding to the very first self-pulsations (the ones that are seen for the lowest values of feedback) follows a tendency very close to f_{RO} when J/J_{th} is varied. This tendency is not seen for the values of f_{SP} corresponding to medium or high feedback regimes, which confirms that the influence of f_{RO} is significant only in weak feedback configurations.

These observations, along with further numerical analysis, allow us to give a general interpretation of the evolution of f_{SP}. The main result that we point out here is that according to the feedback strength, the relative influences of f_{RO} and f_{cav} on f_{SP} vary. They act as two competing parameters causing f_{SP} to describe an evolution within a frequency interval bounded by the two of them, as presented in Fig. 12. The corresponding curve starts with a strong increase from a value slightly larger than f_{RO} and tends to reach the value

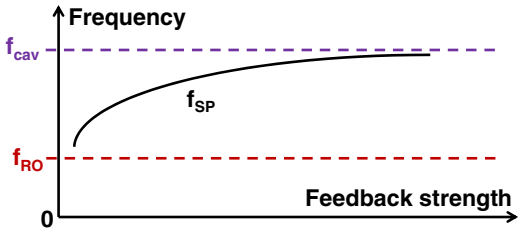

FIG. 12. (Color online) Qualitative interpretation of the general evolution of the self-pulsing frequency with the feedback strength. f_{SP} describes an evolution in a range of frequencies bounded by f_{RO} and f_{cav}.

of f_{cav} at a smoother pace as the feedback strength increases. The existence of a self-pulsing dynamics dominated by the relaxation oscillation frequency at weak feedback and by the external cavity frequency at larger feedback strengths is a known feature of the Lang-Kobayashi model [46]. It is here experimentally measured in the case of a short external cavity.

VII. CONCLUSION

We provide a systematic experimental bifurcation scenario showing self-pulsing dynamics in a laser with short external cavity embedded in a photonic integrated circuit. The dynamical scenario made of cycles of stationary states, self-pulsations of increasing frequency, and quasiperiodicity induced by the increase of the feedback strength is evidenced. Numerical simulations based on the Lang-Kobayashi rate equations provide results in good qualitative agreement with the experimental observations and bring insight into the phenomenon of self-pulsation through mode-antimode beating, originated by bridges between branches of stable and unstable stationary solutions. Despite the simplicity of the model, we unveil a set of parameters under which the dynamical and frequency features show very good compliance with the experimental observations. In addition, we understand that the pulsing frequency is a consequence of an interplay between the frequencies of both the relaxation oscillations and the external cavity. This dynamical specificity to short-cavity lasers is an encouraging step towards both the understanding of PIC behaviors and generation of high-frequency harmonic optical oscillations without the need for electrical modulation and its frequency limitation concerns.

ACKNOWLEDGMENTS

The authors acknowledge support from Grants-in-Aid for Scientific Research from the Japan Society for the Promotion of Science and Management Expenses Grants from the Ministry of Education, Culture, Sports, Science and Technology in Japan. M.S. acknowledges the financial support of the Fondation Supélec, Conseil Régional de Lorraine, Agence Nationale de la Recherche (ANR) through the project TINO (Grant No. ANR-12-JS03-005), FEDER through the projects PHOTON and APOLLO, and the Inter-University Attraction Pole (IAP) program of BELSPO through the project "Photonics@be," Grant No. IAP P7/35.

[1] M. C. Soriano, J. García-Ojalvo, C. R. Mirasso, and I. Fischer, Rev. Mod. Phys. **85**, 421 (2013).
[2] M. Sciamanna and K. A. Shore, Nature Photon. **9**, 151 (2015).
[3] J. S. Cohen, R. R. Drenten, and B. H. Verbeeck, IEEE J. Quantum Electron. **24**, 1989 (1988).
[4] J. Mørk, B. Tromborg, and J. Mark, IEEE J. Quantum Electron. **28**, 93 (1992).
[5] H. Li, J. Ye, and J. G. McInerney, IEEE J. Quantum Electron. **29**, 2421 (1993).
[6] K. Petermann, in *Advanced Networks and Services* (International Society for Optics and Photonics, Amsterdam, 1995), pp. 121–129.
[7] A. Hohl and A. Gavrielides, Phys. Rev. Lett. **82**, 1148 (1999).
[8] H. G. Winful and G. D. Cooperman, Appl. Phys. Lett. **40**, 298 (1982).
[9] C. Bornholdt, B. Sartorius, S. Schelhase, M. Möhrle, and S. Bauer, Electron. Lett. **36**, 327 (2000).
[10] M. Radziunas, H.-J. Wünsche, B. Sartorius, O. Brox, D. Hoffmann, K. R. Schneider, and D. Marcenac, IEEE J. Quantum Electron. **36**, 1026 (2000).
[11] O. Brox, S. Bauer, M. Radziunas, M. Wolfrum, J. Sieber, J. Kreissl, B. Sartorius, and H.-J. Wünsche, IEEE J. Quantum Electron. **39**, 1381 (2003).
[12] S. Bauer, O. Brox, J. Kreissl, B. Sartorius, M. Radziunas, J. Sieber, H.-J. Wünsche, and F. Henneberger, Phys. Rev. E **69**, 016206 (2004).
[13] R. Broom, Electron. Lett. **5**, 571 (1969).
[14] G. Klose and A. Siahmakoun, Opt. Eng. **35**, 2983 (1996).
[15] A. A. Tager and K. Petermann, IEEE J. Quantum Electron. **30**, 1553 (1994).
[16] A. Karsaklian Dal Bosco, D. Wolfersberger, and M. Sciamanna, Appl. Phys. Lett. **105**, 081101 (2014).
[17] T. Sano, Phys. Rev. A **50**, 2719 (1994).
[18] D. Pieroux, T. Erneux, B. Haegeman, K. Engelborghs, and D. Roose, Phys. Rev. Lett. **87**, 193901 (2001).
[19] M. Sciamanna, T. Erneux, F. Rogister, O. Deparis, P. Mégret, and M. Blondel, Phys. Rev. A **65**, 041801 (2002).
[20] T. Erneux, A. Gavrielides, and M. Sciamanna, Phys. Rev. A **66**, 033809 (2002).
[21] O. Ushakov, S. Bauer, O. Brox, H.-J. Wünsche, and F. Henneberger, Phys. Rev. Lett. **92**, 043902 (2004).
[22] T. Heil, I. Fischer, W. Elsäßer, and A. Gavrielides, Phys. Rev. Lett. **87**, 243901 (2001).
[23] A. Tabaka, M. Peil, M. Sciamanna, I. Fischer, W. Elsäßer, H. Thienpont, I. Veretennicoff, and K. Panajotov, Phys. Rev. A **73**, 013810 (2006).
[24] A. Argyris, M. Hamacher, K. E. Chlouverakis, A. Bogris, and D. Syvridis, Phys. Rev. Lett. **100**, 194101 (2008).
[25] A. Argyris, E. Grivas, M. Hamacher, A. Bogris, and D. Syvridis, Opt. Express **18**, 5188 (2010).
[26] A. Argyris, S. Deligiannidis, E. Pikasis, A. Bogris, and D. Syvridis, Opt. Express **18**, 18763 (2010).
[27] T. Harayama, S. Sunada, K. Yoshimura, P. Davis, K. Tsuzuki, and A. Uchida, Phys. Rev. A **83**, 031803 (2011).
[28] S. Sunada, T. Harayama, K. Arai, K. Yoshimura, P. Davis, K. Tsuzuki, and A. Uchida, Opt. Express **19**, 5713 (2011).
[29] R. Takahashi, Y. Akizawa, A. Uchida, T. Harayama, K. Tsuzuki, S. Sunada, K. Arai, K. Yoshimura, and P. Davis, Opt. Express **22**, 11727 (2014).
[30] J. E. Carroll, J. Whiteaway, and D. Plumb, *Distributed Feedback Semiconductor Lasers*, Vol. 10 (IET, London, 1998).
[31] U. Bendelow, M. Radziunas, J. Sieber, and M. Wolfrum, IEEE J. Quantum Electron. **37**, 183 (2001).
[32] J. P. Toomey, D. M. Kane, C. McMahon, A. Argyris, and D. Syvridis, Opt. Express **23**, 18754 (2015).
[33] T. Heil, I. Fischer, W. Elsäßer, B. Krauskopf, K. Green, and A. Gavrielides, Phys. Rev. E **67**, 066214 (2003).
[34] A. Tabaka, K. Panajotov, I. Veretennicoff, and M. Sciamanna, Phys. Rev. E **70**, 036211 (2004).
[35] A. Kaszubowska, P. Anandarajah, and L. P. Barry, IEEE Photonics Technol. Lett. **16**, 605 (2004).
[36] N. Dagli, IEEE Trans. Microwave Theory Tech. **47**, 1151 (1999).
[37] T. Simpson and F. Doft, IEEE Photonics Technol. Lett. **11**, 1476 (1999).
[38] J. Genest, M. Chamberland, P. Tremblay, and M. Têtu, IEEE J. Quantum Electron. **33**, 989 (1997).
[39] S.-C. Chan, S.-K. Hwang, and J.-M. Liu, Opt. Express **15**, 14921 (2007).
[40] S.-C. Chan and J.-M. Liu, IEEE J. Sel. Top. Quantum Electron. **10**, 1025 (2004).
[41] Y.-S. Juan and F.-Y. Lin, IEEE Photon. J. **3**, 644 (2011).
[42] R. Lang and K. Kobayashi, IEEE J. Quantum Electron. **16**, 347 (1980).
[43] J. Ohtsubo, *Semiconductor Lasers: Stability, Instability and Chaos*, Springer Series in Optical Sciences (Springer Verlag, Berlin-Heidelberg, 2008).
[44] A. Uchida, *Optical Communication with Chaotic Lasers: Applications of Nonlinear Dynamics and Synchronization* (Wiley-VCH, Weinheim, 2012).
[45] I. Fischer, G. H. M. van Tartwijk, A. M. Levine, W. Elsäßer, E. Göbel, and D. Lenstra, Phys. Rev. Lett. **76**, 220 (1996).
[46] M. Sciamanna, P. Mégret, and M. Blondel, Phys. Rev. E **69**, 046209 (2004).